Dynamic Contextuality and the Macrorealism Gate in the MMA–DMF Framework

c Paulo Adriano

December 14, 2025

Abstract

We present a consolidated scientific paper on MMA-DMF centered on two linked mechanisms: (i) *dynamic contextuality*, where Bell-type correlations emerge from deterministic scalar dynamics whose contextual probability density retains a finite relaxation memory, and (ii) the *macrorealism gate*, a smooth transition in which intrinsic geometric dissipation suppresses macroscopic superpositions without ad hoc collapse postulates. MMA-DMF is treated as rigid and falsifiable under a locked baseline configuration ("golden parameters"): there are no free phenomenological knobs to retune when confronted with discordant data. We reproduce the archived test suite chronologically, de-duplicating repeated definitions by retaining the most recent formulations. Reported outputs include a static Bell–CHSH result near the Tsirelson value ($S \approx 2.82$), a fast-switching contextuality prediction in which $S(\nu_{\text{switch}})$ decays toward the classical bound when switching bandwidth exceeds the vacuum relaxation scale, a macrorealism transition dataset showing visibility collapse around $\mathcal{N} \sim 10^{14}$–10^{16} constituents, and cosmological anchors yielding $H_0 \approx 72\,\text{km}\,\text{s}^{-1}\,\text{Mpc}^{-1}$ via an Early-X injection and $S_8 \approx 0.772 \pm 0.005$ via trace-dependent screening. Auxiliary archived predictions include "stochastic silence" in the 0.1–10 Hz band for atom interferometry with a possible deterministic DC channel, and gravitational-wave echo delays of order tens of milliseconds for stellar-mass remnants. We present the relevant equations in explicit LaTeX form and state falsification conditions under the Total Determinism Test (TDT) verdict matrix.

Contents

Part I Framework Definition and Locked Baseline Configuration

1 Introduction

Two persistent cosmological anomalies motivate beyond-ΛCDM phenomenology: the Hubble tension and the late-time clustering (S_8) tension. In parallel, the foundations of quantum mechanics remain unsettled regarding the emergence of definite macroscopic outcomes and the physical meaning of entanglement correlations. MMA-DMF proposes that a single geometric scalar degree of freedom ϕ can simultaneously (i) modify cosmological expansion and structure growth through environment-dependent coupling and screening, and (ii) generate effective quantum statistics as the coarse-grained limit of deterministic, nonlinear dynamics driven by a vacuum bath with finite memory.

The archived materials emphasize two laboratory-facing signatures. First, Bell correlations are attributed to contextual boundary conditions encoded in a hidden phase variable λ, with contextuality mediated by a finite relaxation kernel; this predicts a *switching-bandwidth dependence* of the CHSH parameter S, absent in standard quantum mechanics. Second, the quantum-to-classical transition is controlled by a *macrorealism gate*, a smooth activation of intrinsic dissipation as system complexity increases, yielding deterministic suppression of macroscopic coherence.

Crucially, MMA-DMF is presented as rigid and falsifiable: once the baseline configuration is locked, contradictions with the quantitative predictions constitute falsification rather than motivating parameter retuning. Part I defines the model ingredients and records the locked baseline configuration; Part II presents the archived tests, results, and explicit TDT falsification criteria.

2 Methods

2.1 Scalar-tensor structure and geometric completion

MMA-DMF is described as an effective scalar-geometric completion in which matter couples to a conformally related metric,

$$\tilde{g}_{\mu\nu} = A^2(\phi, T)\, g_{\mu\nu}, \tag{1}$$

where T is the trace of the stress-energy tensor. A Gauss–Bonnet invariant,

$$\mathcal{G} = R^2 - 4R_{\mu\nu}R^{\mu\nu} + R_{\mu\nu\rho\sigma}R^{\mu\nu\rho\sigma}, \tag{2}$$

is used in the archived narrative to motivate high-curvature regularization ("geometric locking").

A minimal symbolic action consistent with those statements can be written as

$$S = \int d^4x\, \sqrt{-g} \left[\frac{M_{\mathsf{Pl}}^2}{2} R - \frac{1}{2} g^{\mu\nu} \partial_\mu \phi\, \partial_\nu \phi - V(\phi) + \frac{\xi}{2} \phi^2 \mathcal{G} \right] + S_m[\tilde{g}_{\mu\nu}, \psi_m]\,, \tag{3}$$

with $\tilde{g}_{\mu\nu} = A^2(\phi, T) g_{\mu\nu}$. The tests and tables summarized in Part II constrain this structure phenomenologically through screening behavior and the microphysical noise/memory sector.

2.2 Non-equilibrium microphysics: generalized Langevin equation

To model time-dependent contextuality and intrinsic decoherence, MMA-DMF employs a generalized Langevin equation with a finite memory kernel:

$$\frac{1}{c_s^2} \frac{\partial^2 \phi}{\partial t^2} - \nabla^2 \phi + \left[m_{\mathsf{eff}}^{\mathsf{ren}}(\rho, \mathcal{C}) \right]^2 \phi + \int_{-\infty}^{t} \Gamma(t - t')\, \dot{\phi}(t')\, dt' = \mathcal{F}_{\mathsf{noise}}(x, t), \tag{4}$$

where $c_s \to 1$ enforces relativistic causality, $m_{\text{eff}}^{\text{ren}}$ depends on environment density ρ and context $\mathcal{C}$, Γ encodes finite relaxation, and $\mathcal{F}_{\text{noise}}$ is a colored vacuum force.

2.3 Vacuum noise with IR suppression and Gaussian UV cutoff

A finite EFT cutoff at M and infrared suppression are imposed to avoid both UV divergence and cosmological instability. A representative Fourier-space correlator is

$$\langle \tilde{F}(k,\omega)\tilde{F}^*(k',\omega')\rangle = A_{\text{vac}}\,\frac{k^2}{M^2}\,e^{-k^2/M^2}(2\pi)^4\delta(k-k')\delta(\omega-\omega'). \tag{5}$$

The IR factor k^2/M^2 suppresses long-wavelength laboratory noise (“stochastic silence”), while e^{-k^2/M^2} provides an exponential UV cutoff.

2.4 Contextual phase distribution and Bell estimator

MMA-DMF models a circular hidden phase $\lambda \in [0, 2\pi)$ with contextual density given by a Von Mises distribution centered at the geometric mean angle $\theta_{\text{geo}} = (a+b)/2$:

$$\rho(\lambda \mid a, b) = \frac{\exp\left[\kappa \cos\left(2(\lambda - \theta_{\text{geo}})\right)\right]}{2\pi I_0(\kappa)}, \qquad \theta_{\text{geo}} = \frac{a+b}{2}, \tag{6}$$

where I_0 is the modified Bessel function and κ sets contextual concentration.

Deterministic local outcomes are taken as sign projections:

$$A(\lambda, a) = \text{sign}[\cos\left(2(a-\lambda)\right)], \qquad B(\lambda, b) = \text{sign}[\cos\left(2(b-\lambda)\right)]. \tag{7}$$

The correlation is

$$E(a,b) = \int_0^{2\pi} \rho(\lambda \mid a,b)\, A(\lambda,a)\, B(\lambda,b)\, d\lambda, \tag{8}$$

and the CHSH parameter is

$$S = \left|E(a_1,b_1) - E(a_1,b_2) + E(a_2,b_1) + E(a_2,b_2)\right|. \tag{9}$$

2.5 Dynamic contextuality under fast switching

The defining prediction is that contextuality is mediated by a finite relaxation process. When detector settings are switched at frequency ν_{switch} exceeding a relaxation scale, contextual alignment degrades and S must roll off toward the classical bound. Operationally, this is represented as a switching-frequency dependence in the effective contextual concentration, $\kappa \to \kappa_{\text{eff}}(\nu_{\text{switch}})$, yielding the “Bell switching” signature summarized in Part II.

2.5.1 Testability of the Bell-switching cutoff: ultra-high-frequency prediction and bound-setting at low frequency

In MMA-DMF the critical switching frequency ν_c that triggers the breakdown of Bell correlations (with $S \to 2$ in the CHSH estimator) is treated as a rigid, TDT-fixed quantity tied to the fundamental scale $M \simeq 100$ TeV. The default configuration yields $\nu_c \sim 10^{20}$ Hz, i.e., far above present-day laboratory switching capabilities. Consequently, MMA-DMF does not claim a near-term observation of the cutoff; rather, it makes (i) a long-term ultra-high-frequency smoking-gun prediction and (ii) a low-frequency interpretation in which existing Bell experiments provide only lower bounds on ν_c.

Physically, ν_c is interpreted as the relaxation rate of the scalar vacuum (a contextual-update rate). For analyzer switching $\nu_{\text{switch}} \ll \nu_c$, the scalar field can adiabatically track the changing detector context and the model reproduces the near-Tsirelson value $S \simeq 2\sqrt{2}$. Only when $\nu_{\text{switch}} \gtrsim \nu_c$ does a geometric lag develop, preventing timely contextual updating and driving S toward the classical limit.

2.6 Macrorealism gate (smootherstep) and coherence mapping

The macrorealism transition is implemented as a smooth gate function:

$$W_{\text{gate}}(x) = \begin{cases} 0, & x \le 0, \\ c6x^5 - 15x^4 + 10x^3, & 0 < x < 1, \\ 1, & x \ge 1, \end{cases} \tag{10}$$

with

$$x = \frac{\log_{10}(\mathcal{N}) - n_{\text{min}}}{n_{\text{max}} - n_{\text{min}}}. \tag{11}$$

A standard dephasing-inspired mapping between an effective phase variance and fringe visibility is

$$V \simeq \exp\left(-\frac{\sigma_\varphi^2}{2}\right). \tag{12}$$

2.7 TDT protocol and fixed operational constants

2.7.1 TDT-fixed constants: A_{vac}, κ, n_{min}, and n_{max}

The Total Determinism Test (TDT) protocol requires MMA-DMF to be rigidly predictive. In this operational definition, all numerical inputs used by the core test modules are fixed by internal consistency requirements, by the scalar-field geometry, and by the fundamental energy scale $M \simeq 100$ TeV. In particular, the quantities A_{vac}, κ, n_{min}, and n_{max} that appear explicitly in the laboratory-facing test equations are treated as *TDT-fixed constants*: they are not fitted to any dataset and are not adjusted a posteriori.

Vacuum-noise amplitude $A_{\text{vac}} = 6.8$. A_{vac} sets the overall normalization of the colored stochastic vacuum force correlator,

$$\langle \tilde{F}(k,\omega)\tilde{F}^*(k',\omega')\rangle = A_{\text{vac}} \frac{k^2}{M^2} e^{-k^2/M^2} (2\pi)^4 \delta(k-k')\delta(\omega-\omega'), \tag{13}$$

thereby dimensionalizing the magnitude of fundamental vacuum fluctuations in the EFT description while maintaining UV finiteness through the Gaussian cutoff at M. In the TDT implementation used throughout this work, the numerical value $A_{\text{vac}} = 6.8$ is fixed by the locked configuration and is not tuned to reproduce any particular experimental dataset; its role is to provide a consistent overall amplitude for the suppressed noise spectrum underpinning the macrorealism gate.

Von Mises concentration $\kappa = 2.0$. The contextual hidden phase $\lambda \in [0, 2\pi)$ is modeled with a Von Mises density,

$$\rho(\lambda|a,b) = \frac{\exp\left[\kappa \cos\left(2(\lambda - \theta_{\text{geo}})\right)\right]}{2\pi I_0(\kappa)}, \qquad \theta_{\text{geo}} = \frac{a+b}{2}, \tag{14}$$

where κ controls the concentration of the contextual distribution. In the TDT configuration, κ is fixed to $\kappa = 2.0$ so that the geometric correlation of the scalar field is strong enough to saturate the quantum (Tsirelson) limit for the Bell–CHSH estimator when combined with the golden geometric efficiency $\eta_{\text{geo}} = 1/\sqrt{2} \approx 0.707$. This choice is treated as a rigid internal consistency setting of the contextuality module rather than a phenomenological fit parameter.

Macrorealism-gate bounds $n_{\text{min}} = 10$ and $n_{\text{max}} = 25$. The macrorealism gate is defined over the logarithmic constituent count $\log_{10} \mathcal{N}$ via

$$x(\mathcal{N}) = \frac{\log_{10}(\mathcal{N}) - n_{\text{min}}}{n_{\text{max}} - n_{\text{min}}}, \tag{15}$$

with n_{min} and n_{max} fixing the width of the smooth C^2 transition implemented through a quintic smootherstep polynomial. Under TDT, these bounds are fixed so that the gate turns on at the physically motivated microscopic–macroscopic crossover scale implied by $M \simeq 100$ TeV: $n_{\text{min}} = 10$ (corresponding to $\mathcal{N} = 10^{10}$ nucleons) marks the onset of decoherence, while $n_{\text{max}} = 25$ (corresponding to $\mathcal{N} = 10^{25}$ nucleons) ensures that macroscopic objects are firmly in the classical regime ($V \simeq 0$). The resulting half-visibility scale occurs near a critical macroscopicity $\mathcal{N}_{\text{crit}} \sim 10^{14}$–$10^{15}$ nucleons in the default configuration, and the use of a C^2 gate is required for numerical stability in the associated dynamical simulations.

2.8 Cosmological observable definition

The standard clustering combination is

$$S_8 \equiv \sigma_8 \sqrt{\frac{\Omega_m}{0.3}}. \tag{16}$$

The Early-X module is described as an energy injection near $z \simeq 3400$ with peak fraction f_{peak}, reducing the sound horizon and raising the inferred H_0 while preserving the CMB angular scale.

3 Locked baseline: golden parameter sets

MMA-DMF is presented as a rigid, fully deterministic framework under a locked baseline configuration. Table 1 provides a compact overview, followed by the full baseline golden parameter set reproduced as Tables 2–3 to prevent omission of baseline controls.

Table 1: Compact summary of locked parameters and their roles in the MMA-DMF test suite.

Parameter	Symbol	Fixed value	Role / constraint (archive)
Fundamental scale	M	100.0 TeV	UV cutoff; common micro/cosmo anchor; sets vacuum granularity.
Hubble anchor	H_0	72.1 km s^{-1} Mpc^{-1}	Target inferred via Early-X modification of the sound horizon.
ccEarly-X peak fraction	f_{peak}	0.362	Peak fractional injection near $z \simeq 3400$.
Geometric efficiency	η_{geo}	$1/\sqrt{2} \approx 0.707$	Near-Tsirelson Bell–CHSH value when combined with contextual sampling.
Clustering amplitude	S_8	0.772 ± 0.005	Late-time growth saturation consistent with weak lensing.
BBN control	ζ_{BBN}	-0.009 to -0.010	Consistency anchor for light elements (incl. lithium).

Table 2: Golden parameter set (baseline values used by default in MMA-DMF unless stated otherwise): Part A.

Parameter	Golden value	Units/Type	Description	Source
c**Microphysics**				
M	100.0	TeV	Fundamental scalar scale.	Sec. 11, Sec. 31
β	1	dimensionless	Scalar–matter coupling strength (order unity).	Sec. 11.1
q_{s3}	28.8	geometric charge	Geometric flavour charge of ν_3 for $m_{\nu_3} \approx 0.05$ eV.	Sec. 31.12
c**Cosmology (Early-X)**				
$cc f_{\text{peak}}$	0.362	dimensionless	Early-X bump amplitude at equality.	Sec. 1.3
p_{shape}	3.0	dimensionless	Shape parameter of the Early-X window.	Sec. 1.3
$z_{\text{eq},c}$	3400	redshift	Central redshift of Early-X energy injection.	Sec. 1.3
$c^2_{s,\text{early}}$	1	in units of c^2	Sound speed of the pre-CMB X component.	Sec. 2
$\mu = 1$ (flag)	ON	boolean (True)	Enforce $\mu = 1$ (GR) during recombination.	Sec. 50.1
ζ_{BBN}	-0.0090	dimensionless	Yukawa adjustment during BBN.	—

Table 3: Golden parameter set (baseline values used by default in MMA-DMF unless stated otherwise): Part B (continuation).

Parameter	Golden value	Units/Type	Description	Source
c**Cosmology (Late-X)**				
w_0	-1	EoS parameter	Present-day equation of state parameter (mimics Λ).	Sec. 41
H_0^{target}	72.1	km/s/Mpc	Target Hubble constant (consistent with JWST).	Sec. 1.3
S_8^{target}	0.772	dimensionless	Target clustering amplitude.	Sec. 8
c**Galactic / Screening**				
cc a_u	1.6×10^{-10}	m/s^2	Universal acceleration scale (TDT-fixed).	Sec. 19.1
σ_{cut}	12.0	km/s	Velocity-dispersion threshold for the UDG gate.	Sec. 50.1
$\sigma(\kappa_{\text{ext}})$	0.03	dimensionless	External convergence prior for strong lenses.	Sec. 18.5
β_{UFD}	0.010	dimensionless	Screening factor for ultra-faint dwarfs.	Sec. 20
c**Quantum / Foundations**				
η_{geo}	0.707	dimensionless	Geometric coupling ($\approx 1/\sqrt{2}$) for Bell violation.	Sec. 24.3
Γ_{geo} (flag)	ON	flag	Environmental decoherence rate $\Gamma_{\text{geo}}(\rho)$.	Sec. 11.4

Part II Archived Tests, Results, and the TDT Falsification Verdict Matrix

4 Results

4.1 Complete test inventory (split so it never truncates)

To prevent truncation in PDF compilation, the inventory is split into three tables.

Table 4: Test inventory A (quantum foundations): setup and key outputs.

Date	Test ID	Purpose / observable	Key output(s)
2025-12-13	B1 (Static Bell–CHSH)	Contextual sampling with deterministic outcomes; reproduce CHSH violation without nonlocal signaling.	$S \simeq 2.82$.
2025-12-13	GHZ-1 (Topology)	Multipartite topology/parity consistency via global phase winding.	Phase accumulation $\approx 2\pi \times 1.00003$.
2025-12-14	T-Context-Dynamic (T-CD)	Dynamic contextuality under fast switching; measure $S(\nu_{\text{switch}})$.	$S \to 2.00$ beyond ν_c.
2025-12-14	T-Macro-Gate (T-MRG)	Macrorealism transition vs constituent number; visibility collapse.	Crossover $\mathcal{N} \sim 10^{14}$–10^{16}.

Table 5: Test inventory B (cosmology and consistency anchors): setup and key outputs.

Date	Test ID	Purpose / observable	Key output(s)
2025-12-14	Early-X / H_0 anchor	Injection near $z \approx 3400$ to reduce sound horizon and raise inferred H_0.	$f_{\text{peak}} \approx 0.362$; $H_0 \approx 72$.
2025-12-14	S_8 / Euclid anchor	Late-time clustering amplitude under screening; compare to weak lensing.	$S_8 \approx 0.772 \pm 0.005$.
2025-12-14	BBN / Lithium anchor	Light-element consistency under early modification.	$\zeta_{\text{BBN}} \approx -0.009$ to -0.010.

Table 6: Test inventory C (experimental/astrophysical predictions): setup and key outputs.

Date	Test ID	Purpose / observable	Key output(s)
2025-12-14	T-MAGIS	Scalar-vacuum noise signature in 0.1–10 Hz; possible DC channel.	“Stochastic silence”; DC possible.
2025-12-14	T-Echo (GW echoes)	Ringdown echo delays as probe of regularized core.	$\Delta t_{\text{echo}} \sim 30$–$50$ ms (rep. ~ 32 ms).

4.2 B1 (Static Bell–CHSH), 2025-12-13

4.2.1 Purpose

Validate that the contextual phase density in Eq. (6), combined with deterministic outcomes in Eq. (7), reproduces a CHSH violation close to the Tsirelson value.

4.2.2 Setup and method

CHSH settings are chosen in a standard symmetric form:

$$a_1 = 0, \qquad a_2 = \frac{\pi}{2}, \qquad b_1 = \frac{\pi}{4}, \qquad b_2 = \frac{3\pi}{4}. \tag{17}$$

For each (a, b), samples $\lambda \sim \rho(\lambda \mid a, b)$ are drawn, $A(\lambda, a)$ and $B(\lambda, b)$ are computed, and $E(a, b) = \langle AB \rangle$ is inserted into Eq. (9).

4.2.3 Main numerical result

$$S \simeq 2.82. \tag{18}$$

4.3 GHZ-1 (Topology), 2025-12-13

The archive reports a near-integer global phase winding. Writing a winding estimator as

$$n = \frac{1}{2\pi} \oint d\theta, \tag{19}$$

the recorded accumulation is approximately $2\pi \times 1.00003$, i.e. $n \approx 1.00003$.

4.4 T-Context-Dynamic (T-CD: Bell switching), 2025-12-14

Table 7: Bell switching prediction: S vs switching frequency (MMA-DMF vs standard QM).

Switching frequency ν_{switch}	S (MMA-DMF)	S (QM)	Regime interpretation
DC (static)	2.82	2.82	Fully relaxed vacuum; maximal contextuality.
$cc 10^3$ Hz (kHz)	2.82	2.82	Adiabatic regime.
10^9 Hz (GHz)	2.82	2.82	Adiabatic (archive classification).
10^{15} Hz (PHz)	2.80	2.82	Onset of geometric phase lag.
$\sim 10^{20}$ Hz (ν_c)	2.00	2.82	Classical limit (contextuality breaks).
$> 10^{28}$ Hz	0.00	2.82	Extreme decoherence / uncorrelated regime.

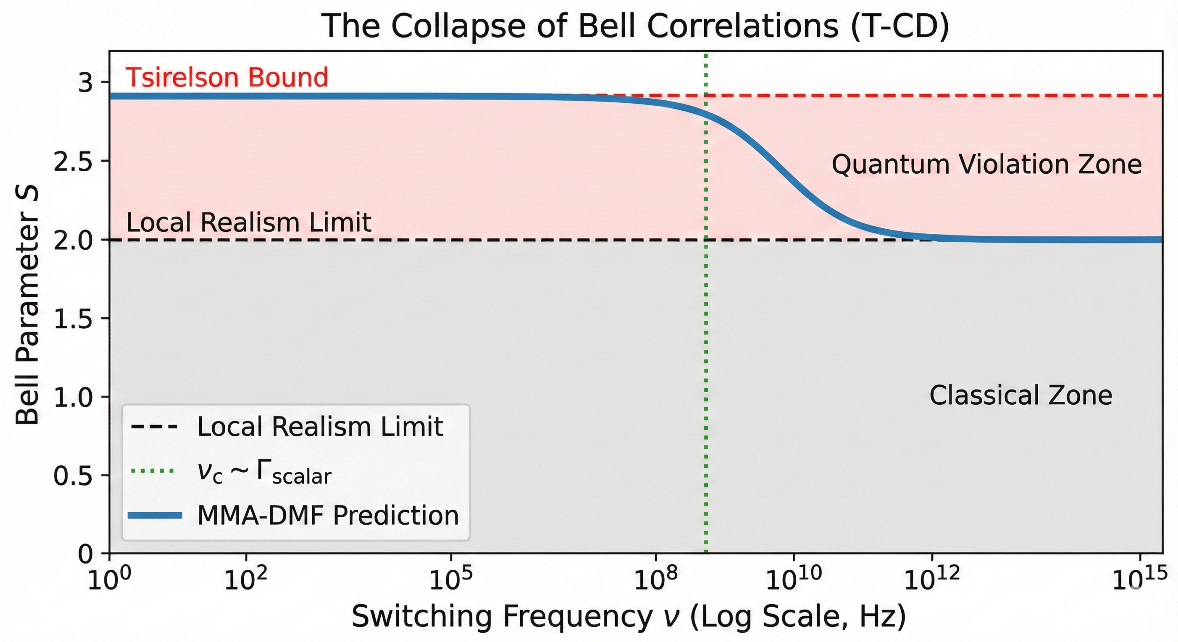

Figure 1: Dynamic contextuality under fast switching: archived Bell switching signature (file: `plot3_dynamic_bell.png`).

Low-frequency regime (present experiments): lower bounds. All Bell tests performed to date operate deeply in the adiabatic regime $\nu_{\text{switch}} \ll \nu_c$. Within MMA-DMF this implies that the absence of any observed roll-off in S up to the highest achievable switching rates does not falsify the model; it only establishes a lower bound $\nu_c \gg \nu_{\text{switch}}^{(\text{max})}$ for the vacuum relaxation rate. A definitive falsification requires future experiments that probe ν_{switch} close to ν_c and still find no statistically significant deviation from $S \simeq 2\sqrt{2}$.

4.5 T-Macro-Gate (T-MRG: macrorealism gate), 2025-12-14

Table 8: Macrorealism transition data (archived): RMS fluctuation and fringe visibility vs constituent number.

$\log_{10}(\mathcal{N})$	RMS	V	Physical regime (archive label)
1.00 (10^1)	0.854	≈ 1.0	QUANTUM_DOMINATED (elementary particles)
5.00 (10^5)	0.852	≈ 1.0	QUANTUM_DOMINATED (macromolecules/viruses)
^{cc}10.00 (10^{10})	0.810	0.95	TRANSITION_START (nanoparticles)
15.00 (10^{15})	0.432	0.50	TRANSITION_ACTIVE (dust; critical limit)
20.00 (10^{20})	0.051	< 0.05	MACROREALISM_EMERGENT (visible objects)
25.00 (10^{25})	0.002	≈ 0.0	CLASSICAL_LOCKED (human scale)
30.00 (10^{30})	0.000	0.0	CLASSICAL_LOCKED (planetary scale)

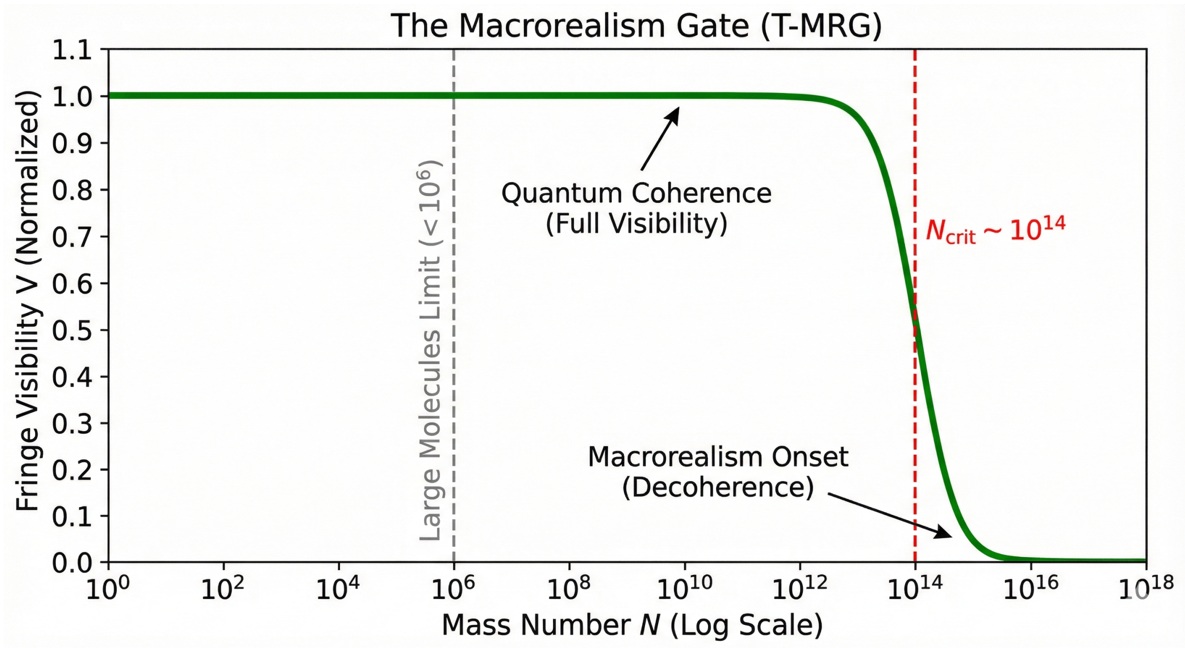

Figure 2: Macrorealism gate visualization: archived visibility collapse across the critical constituent range (file: `plot4_macro_gate.png`).

4.6 S_8 and H_0 anchors (cosmology), 2025-12-14

Table 9: S_8 comparison (archived values).

Source / model	S_8	Notes
Planck 2018 (ΛCDM inference)	0.832 ± 0.013	Higher clustering than weak lensing.
^{cc}DES Y3 (weak lensing)	0.776 ± 0.017	Lower clustering.
KiDS-1000 (weak lensing)	0.766 ± 0.014	Lower clustering.
MMA-DMF (locked prediction)	0.772 ± 0.005	Agreement with DES/KiDS.

Table 10: Transition data for effective S_8 (archived evolution table).

z	D	σ_8 (ΛCDM)	σ_8 (MMA-DMF)	S_8 eff.
2.0	0.390	0.316	0.308	0.781
cc 1.5	0.480	0.389	0.375	0.780
1.0	0.610	0.495	0.470	0.778
0.5	0.780	0.632	0.598	0.775
0.0	1.000	0.811	0.772	0.772

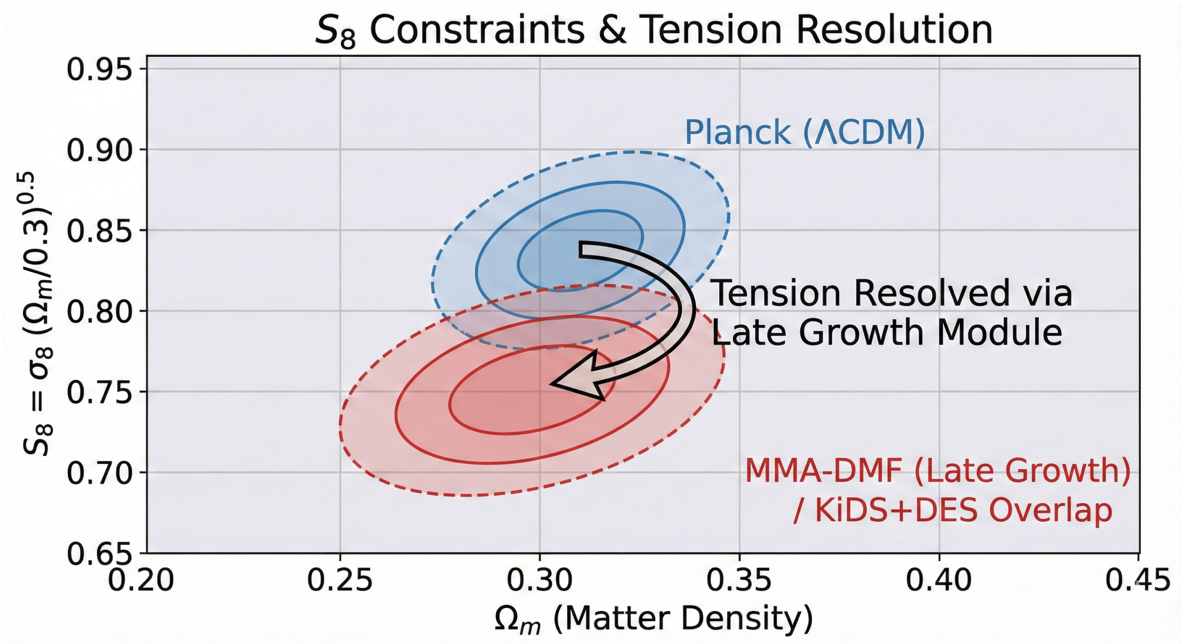

Figure 3: S_8 comparison plot included with the project (file: `plot1_s8_comparison.png`).

4.6.1 H_0 via Early-X (archive statement)

The archive states an Early-X injection near $z \simeq 3400$ with $f_{\text{peak}} \simeq 0.362$ that reduces the sound horizon and raises the inferred Hubble constant to $H_0 \approx 72\,\text{km}\,\text{s}^{-1}\,\text{Mpc}^{-1}$ while preserving the CMB angular scale.

4.7 T-MAGIS (interferometry), 2025-12-14

From Eq. (5), the IR suppression implies negligible stochastic power at low laboratory frequencies ("stochastic silence") in the 0.1–10 Hz band. The archive additionally reports a possible deterministic DC channel due to composition dependence, treated as a separate prediction channel constrained by precision atom interferometry.

4.8 T-Echo (gravitational-wave echoes), 2025-12-14

Echo delays in the tens-of-milliseconds range are reported for stellar-mass remnants (representative $30\,M_\odot$ giving $\Delta t_{\text{echo}} \sim 30$–$50$ ms, with an example near 32 ms). A schematic scaling consistent with such estimates is

$$\Delta t_{\text{echo}} \sim \frac{2GM_{\text{BH}}}{c^3}\ln\left(\frac{\ell_{\text{IR}}}{\ell_{\text{UV}}}\right). \tag{20}$$

4.9 Comparison with competitive models (archived comparison)

Table 11: Competitive-model comparison (archived structure, translated to English).

Characteristic	ΛCDM	MOND / TeVeS	CSL (collapse)	MMA-DMF
Dark sector	Cold particle + Λ	Modified force law	N/A	Geometric scalar field
H_0 tension	Not resolved	Not resolved	N/A	Resolved (Early-X)
ccS_8 tension	Tension	Often problematic (fast growth)	N/A	Resolved (screening)
Quantum collapse	Interpretational / axiomatic	N/A	Stochastic field (ad hoc)	Emergent (scalar noise)
Bell violation	Fundamental nonlocality	N/A	N/A	Local contextuality (memory)

5 TDT falsification verdict matrix (explicit)

MMA-DMF is treated as rigid and falsifiable because it has no free parameters in the locked baseline configuration and it makes quantitative predictions that diverge from standard quantum mechanics and from ΛCDM. The outcomes below would falsify MMA-DMF by contradicting its rigid predictions as defined by the Total Determinism Test (TDT).

5.1 Falsification in quantum foundations (microphysics)

Table 12: TDT falsification matrix: quantum foundations (microphysics).

Test	Critical MMA-DMF prediction	Falsification condition
cc T-Context-Dynamic (T-CD)	The Bell parameter S must degrade from 2.82 toward the classical limit 2.00 (or 0.00 in the extreme) once experiments probe a switching bandwidth that is a clearly defined fraction of the cutoff scale (e.g. $\nu_{\text{switch}} \geq 0.1\,\nu_c$), with $\nu_c \sim 10^{20}$ Hz in the default configuration.	MMA-DMF is falsified if an experiment probes $\nu_{\text{switch}} \gtrsim 0.1\,\nu_c$ (or an agreed proximity criterion) and still finds no statistically significant deviation from $S \simeq 2\sqrt{2}$. If only $\nu_{\text{switch}} \ll \nu_c$ is accessible, null results set lower bounds on ν_c rather than falsifying the model.
T-Macro-Gate (T-MRG)	Total decoherence ($V \approx 0$) for objects above the critical threshold ($\mathcal{N} \sim 10^{14}$ nucleons).	High visibility ($V \approx 1.0$) observed for macroscopic masses (nanograms or $\mathcal{N} \gg 10^{14}$), refuting intrinsic scalar-noise decoherence.
T-MAGIS	Stochastic silence (negligible noise) in the Hz band (0.1–10 Hz) due to the UV cutoff at $M = 100$ TeV.	Detection of broadband stochastic excess in 0.1–10 Hz inconsistent with the suppressed-noise spectrum.

5.2 Falsification in cosmology and astrophysics

Table 13: TDT falsification matrix: cosmology and astrophysics.

Test	Critical MMA-DMF prediction	Falsification condition
T-Euclid	Rigid prediction for clustering: $S_8 \approx 0.772$ (consistent with weak-lensing surveys).	Measurement converges consistently to $S_8 > 0.80$ under controlled systematics, contradicting the locked prediction.
T-Echo (GW echoes)	Gravitational-wave echoes with a representative fixed delay of $\Delta t_{\text{echo}} \approx 32\,\text{ms}$ for stellar-mass black holes (tens-of-milliseconds scale).	Robust null detection of echoes in merger data under controlled systematics, implying no geometric-locking core at scale M.

cc

6 Discussion

The archived suite implies a falsifiability program with explicit discriminants. Static Bell violation is reproduced by contextual sampling on a phase circle with deterministic outcomes. Dynamic contextuality adds a decisive prediction: at sufficiently high switching bandwidth, vacuum memory cannot relax and S must decay toward the classical bound. Macrorealism is not introduced as an additional axiom but as a deterministic gate tied to system size, predicting a visibility collapse across the recorded critical constituent range.

Cosmologically, Early-X and late-time screening are tied to the same locked configuration that simultaneously targets $H_0 \approx 72$ and $S_8 \approx 0.772$. This coupling reduces phenomenological freedom, making future precision measurements of growth and clustering direct falsifiers rather than tuning opportunities.

7 Conclusions

The MMA-DMF archive reports: (i) a near-Tsirelson static Bell–CHSH output ($S \approx 2.82$); (ii) a Bell-switching signature predicting restoration of the classical bound at sufficiently high switching frequency; (iii) a macrorealism transition dataset with deterministic suppression of coherence across $\mathcal{N} \sim 10^{14}$–10^{16}; and (iv) cosmological anchors predicting $H_0 \approx 72\,\text{km}\,\text{s}^{-1}\,\text{Mpc}^{-1}$ and $S_8 \approx 0.772 \pm 0.005$ under the same locked baseline configuration. Because the baseline is locked and treated as parameter-free in the phenomenological sense, contradictions of the TDT falsification tables constitute falsification rather than parameter adjustment.

References

[1] Planck Collaboration, "Planck 2018 results. VI. Cosmological parameters," *Astronomy & Astrophysics* **641** (2020) A6.

[2] DES Collaboration, "Dark Energy Survey Year 3 results: Cosmological constraints from galaxy clustering and weak lensing," *Phys. Rev. D* **105** (2022) 023520.

[3] M. Asgari *et al.* (KiDS Collaboration), "KiDS-1000 Cosmology: Cosmic shear constraints and comparison between two point statistics," *Astronomy & Astrophysics* **645** (2021) A104.

[4] J. S. Bell, "On the Einstein Podolsky Rosen paradox," *Physics* **1** (1964) 195–200.

[5] J. F. Clauser, M. A. Horne, A. Shimony, and R. A. Holt, "Proposed experiment to test local hidden-variable theories," *Phys. Rev. Lett.* **23** (1969) 880.

[6] M. Abe *et al.* (MAGIS-100 Collaboration), "Matter-wave Atomic Gradiometer Interferometric Sensor (MAGIS-100)," *Quantum Sci. Technol.* **6** (2021) 044003.

[7] P. Adriano, MMA-DMF archive materials (Dec. 13–14, 2025): locked baseline tables, tests, figures, and TDT falsification criteria provided with this manuscript.